ECM-integrin signalling instructs cellular position-sensing to pattern the early mouse embryo

Esther Jeong Yoon Kim [1,2], Lydia Sorokin[3], and Takashi Hiiragi[1,4]*

[1] European Molecular Biology Laboratory (EMBL), Heidelberg, Germany
[2] Collaboration for joint PhD degree between EMBL and Heidelberg University, Faculty of Biosciences, Universität Heidelberg, Heidelberg, Germany
[3] Institute of Physiological Chemistry and Pathobiochemistry and Cells in Motion Interfaculty Centre (CiMIC), University of Muenster, Germany
[4] Institute for the Advanced Study of Human Biology (WPI-ASHBi), Kyoto University, Kyoto, Japan

*Correspondence should be addressed to T.H. (hiiragi@embl.de).

Summary statement

This study highlights the importance of patterned cell-extracellular matrix (ECM) interactions in early mouse development, as ECM signals can modulate both cell fate and the relative spatial arrangement between cells.

Abstract

Development entails patterned emergence of diverse cell types within the embryo. In mammals, cells positioned inside the embryo give rise to the inner cell mass (ICM) that eventually forms the embryo proper. Yet the molecular basis of how these cells recognise their 'inside' position to instruct their fate is unknown. Here we show that provision of extracellular matrix (ECM) to isolated embryonic cells induces ICM specification and alters subsequent spatial arrangement between epiblast (EPI) and primitive endoderm (PrE) cells that emerge within the ICM. Notably, this effect is dependent on integrin β1 activity and involves apical to basal conversion of cell

polarity. We demonstrate that ECM-integrin activity is sufficient for 'inside' positional signalling and it is required for proper EPI/PrE patterning. Our findings thus highlight the significance of ECM-integrin adhesion in enabling position-sensing by cells to achieve tissue patterning.

Key words: early mammalian development, extracellular matrix, cell fate specification, patterning

Introduction

Development begets an immense diversity of animal forms as fertilisation is followed by organisation of cells into higher order structures. The emergence of complex patterns generally requires that cells continuously exchange signals with their surroundings to direct their fate and spatial orientation. While transcriptional networks inform individual cell types, the *position* at which a cell lies is critical for tissue patterning. Therefore, relays of spatial information are a ubiquitous requirement in developing systems, and a cell has to sense its position relative to its neighbours to support robust patterning. A cell may glean positional information from a variety of sources, such as mechanochemical gradients, wave-like propagation of signalling activity, as well as direct adhesive interactions with the immediate environment (Jouve et al., 2002; Steinberg and Poole, 1981; Wolpert, 1969).

In particular, adhesive interactions with the extracellular matrix (ECM) are dynamically engaged during development and homeostatic turnover of tissues (Gattazzo et al., 2014; Walma and Yamada, 2020). The ECM consists of a network of various components such as laminin, collagen IV, and fibronectin, which serve to regulate cell behaviours ranging migration, polarisation, survival, and differentiation. Its significance is evident during development, where loss of laminin chains, collagen IV, or their respective receptors leads to early embryonic lethality in mice (Miner et al., 1998; Miner et al., 2004; Smyth et al., 1999; Williamson et al., 1997). Furthermore, laminin regulates gene expression and spatial organisation of cells in several epithelial tissues (Klein et al., 1988; Streuli et al., 1995). In the gut, its loss leads to epithelial hyperplasia and an impaired stem cell pool, while provision of

ECM through Matrigel supports long-term culture of intestinal crypt organoids (Fields et al., 2019; Sato et al., 2009). Similarly, laminin is required for proper positioning and maintenance of follicle stem cells in their niche within the *Drosophila* ovary (O'Reilly et al., 2008). As such, laminin as well as other ECM components have a conserved role in modulating the spatial organisation and behaviour of cells across diverse contexts.

The preimplantation mouse embryo is remarkable in its regulative capacity to preserve embryonic patterning against drastic reduction in cell number (Solter and Knowles, 1975; Tarkowski, 1959; Tarkowski and Wróblewska, 1967). This implies dynamic readout of positional information by blastomeres to adjust their fate and spatial arrangement in response to perturbations. By the end of the preimplantation stage at embryonic day (E) 4.5, the embryo consists of an outermost trophectoderm (TE) monolayer enclosing a fluid-filled cavity and an inner cell mass (ICM). Within the ICM, the primitive endoderm (PrE) forms an epithelial monolayer lining the cavity, while epiblast (EPI) cells reside between the PrE and the overlying polar TE.

Cell position instructs the first lineage segregation in mouse development, as inner and outer cells become ICM and TE, respectively (Rossant and Tam, 2009; Tarkowski and Wróblewska, 1967). Prior to TE specification, the outer surface of the 8-cell embryo is marked by a polarised cortical domain enriched in phosphorylated ezrin, radixin, moesin (pERM), Par6, and atypical protein kinase C (aPKC) (Ducibella et al., 1977; Louvet et al., 1996; Vinot et al., 2005; Ziomek and Johnson, 1980). This apical domain is both necessary and sufficient for TE fate, and effectively serves as the ‘outside’ positional signal to prompt subsequent embryonic patterning (Alarcon, 2010; Korotkevich et al., 2017). Conversely however, insights into specification of the ICM, which gives rise to the embryo proper, thus far remain sparse.

In contrast to apically polarised outer cells, inner cells are separated from the external environment and instead enclosed by adhesive interactions with neighbouring cells. The earliest marker of ICM specification is the upregulation of *Sox2* within these inner cells of the embryo (Guo et al., 2010; Wicklow et al., 2014). Upon perturbation of internalisation or exposure to the external environment, early blastomeres default to a TE-like state (Korotkevich et al., 2017; Lorthongpanich et al., 2012; Stephenson et al., 2010; Tarkowski and Wróblewska, 1967), demonstrating that inside-positioning of the blastomere is crucial for ICM specification.

Results

Integrin and laminin chains are localised at the cell-cell interface

To study the ICM-inducing effects of the embryonic interior, we first examined proteins enriched at the cell-cell interface within the embryo. E-cadherin is clearly localised to cell-cell contact sites from the morula to blastocyst stages, away from TE-associated apical domains enriched in pERM (Figure 1A and 1B). While E-cadherin is the major adhesive molecule that holds cells together irrespective of their fate (Filimonow et al., 2019; Larue et al., 1994; Shirayoshi et al., 1983; Stephenson et al., 2010), several studies have shown that ECM components are also present during this period of development (Dziadek and Timpl, 1985; Leivo et al., 1980; Morin and Sullivan, 1994; Sutherland et al., 1993). However, their significance is little understood.

We found that several laminin chains are enriched at the cell-cell interface in the morula and the ICM region of the blastocyst (Figure 1A and 1B). Immunostaining indicated expression of laminin 511 in addition to the already reported laminin 111, which are heterotrimers of constituent α5, β1, γ1 and α1, β1, γ1 chains, respectively (Cooper and MacQueen, 1983; Leivo et al., 1980; Miner et al., 2004; Smyth et al., 1999). Accordingly, subunits of the major laminin receptor, integrin α6β1, which binds both laminin 111 and 511, were similarly expressed in the preimplantation embryo (Figure 1A and 1B) (Sutherland et al., 1993; Takizawa et al., 2017; Yamada and Sekiguchi, 2015). Close spatial association between laminin and integrin β1 fluorescence around inner cells identified ECM-integrin interactions as candidate ‘inside’ positional signals to blastomeres that could drive ICM specification (Figure 1C and 1D).

Exogenous ECM drives ICM specification and surface integrin α6β1 enrichment

To test whether the ECM can present ‘inside’ positional signals to drive ICM specification, we sought to mimic the inner environment of the embryo by providing ECM to cells through Matrigel, which is rich in laminin 111(Orkin et al., 1977; Timpl

et al., 1979). Embryos were recovered at the morula stage prior to marked upregulation of *Sox2* in inner cells, and TE-specified outer cells were removed by immunosurgery (Figure 2A). Immunosurgery not only isolates naïve inner cells, but also alters their positional identity by exposing them to the external environment (Solter and Knowles, 1975). Subsequent culture of these cells in standard embryo media (KSOM) fully restored inside-outside patterning. CDX2-positive TE cells surrounded SOX2-positive ICM cells and often a small fluid-filled cavity, reminiscent of blastocysts (Figure 2B, top panel). In this way, these isolated cells displayed robust regulative capacity by restoring embryonic patterns seen in whole counterparts.

In stark contrast, however, the TE layer was not restored in the presence of Matrigel. Instead, isolated cells formed a compact mass where the majority of nuclei were SOX2-positive, irrespective of cell position (Figure 2B). CDX2-positive cells were fewer and clustered at the periphery, while fluid-filled cavities were noticeably absent. Moreover, samples entirely composed of SOX2-positive cells were also observed across independent experiments, albeit at low frequency (9 out of 97, 9.3 %) (Figure 2B, bottom panel). Total cell numbers were comparable between the two conditions (Figure 2C), indicating that Matrigel does not have adverse effects on cell survival or proliferation.

Besides expression of *Cdx2* and *Sox2*, TE and ICM cells are distinguishable by differential Hippo signalling (Nishioka et al., 2009; Wicklow et al., 2014). In inner cells, Hippo signalling results in phosphorylation and cytoplasmic retention of YAP. In outer cells, Hippo signalling is inactive, and YAP translocates to the nucleus to drive downstream transcription of *Cdx2*. Consistent with increased *Sox2* expression, nuclear YAP localisation was diminished in Matrigel culture (Figure S1A). Furthermore, quantitative analysis of individual nuclei for levels of each fate marker confirmed significant increase in *Sox2* expression in Matrigel (Figure 2D). These findings demonstrate that exogenously supplied ECM provides ‘inside’ positional cues sufficient to drive ICM specification following immunosurgery even in cells that are physically positioned ‘outside’.

Earlier studies noted that TE specification is preceded by ready polarisation of the outer surface after perturbations such as immunosurgery (Stephenson et al., 2010; Wigger et al., 2017). In agreement to this, pERM was enriched on the outer surface of isolated cells cultured in KSOM, while integrin β1 was limited to cell-cell

interfaces (Figure 2E, top panels). Distinct and mutually exclusive localisation of pERM and integrin β1 is consistent with the apicobasal polarity that accompanies inside-outside patterning in the whole embryo. In contrast, however, Matrigel led to significant enrichment of integrin β1 on the outer surface whereas peripheral pERM was significantly diminished (Figure 2E, bottom panels, 2G and 2H). Discontinuous patches of pERM were sometimes present on the surface, which generally coincided with CDX2-positive or SOX2-negative nuclei (Figure S1B). Integrin α6 localisation was comparable to integrin β1 (Figure 2F), while E-cadherin was limited to cell-cell interfaces regardless of culture conditions (Figure S1C). These suggests that Matrigel, particularly its constituent laminin, brings its receptor integrin α6β1 to the surface in lieu of apical polarity proteins, befitting 'inside' cells.

While ICM cells are roughly isotropic in shape, TE cells are generally oblong under control conditions as these are stretched around the ICM or the fluid-filled cavity (Chan et al., 2019; Niwayama et al., 2019). However, Matrigel abrogated this difference in circularity between TE and ICM cells. The presence of round TE cells in Matrigel culture suggests that fate specification in this setting is not dependent on cell shape (Figure 2I).

Integrin β1 activity is required for ECM-induced ICM specification

To test whether the activity of surface enriched integrin α6β1 is actually required for ICM induction by Matrigel, integrin β1 was inhibited with a function-blocking antibody, Ha2/5 (Mendrick and Kelly, 1993). Administration of Ha2/5 almost completely attenuated the aforementioned effects of Matrigel. Outer cells polarised and became TE specified, while ICM specification was confined to inner cells (Figure 3A, 3B and S2A). In this way, cells cultured in Matrigel with Ha2/5 were indistinguishable from control samples. Similar observations were made upon inhibition of integrin α6 and assessment of YAP localisation (Figure S2B and S2C) (Sonnenberg et al., 1987), where a continuous outer TE layer was restored despite the presence of Matrigel.

Furthermore, upon genetic ablation of *Itgb1*, integrin β1-deficient cells were refractory to the effects of Matrigel (Raghavan et al., 2000). Unlike cells isolated from *Itgb1*$^{+/-}$ littermate controls that exhibited increased ICM specification in Matrigel, inside-outside patterning was restored among *Itgb1*$^{-/-}$ cells (Figure 3C). These indicate that 'inside' positional signals provided by the ECM require recognition through integrin α6β1 activity to drive ICM specification.

Integrin β1 activity is not required for initial specification of ICM but required for EPI-PrE patterning *in vivo*

Earlier observation of integrin β1 mutant mice showed embryonic lethality post-implantation but apparently normal development through the preimplantation stage (Fässler and Meyer, 1995). Accordingly, we found TE-ICM patterning and overall morphology to be comparable between wildtype (WT) and *Itgb1*$^{-/-}$ embryos during most of the preimplantation stage (Figure 4A). Examination of morula stage embryos specifically for presence of the active conformation of integrin β1 revealed that integrin is mostly active on the basal side of outer cells (Figure S3A) (Bazzoni et al., 1995; Humphries et al., 2005). These data consistently suggest that while an abundance of ECM signals is sufficient to drive increased ICM specification as shown earlier, it is not strictly required for TE/ICM patterning *in vivo*.

However, defects were observed upon close examination of mutant blastocysts towards the end of the preimplantation stage around E4.0. Within the mature ICM of a WT blastocyst, PrE cells form an epithelial monolayer that is apically polarised towards the blastocyst cavity, while EPI cells are sheltered between the PrE and the overlying polar TE (Figure 4A). The respective numbers of EPI and PrE cells were not significantly affected by integrin β1 deficiency on average (Figure 4B). On rare occasions, we observed *Itgb1-/-* blastocysts with severe disruption of the ICM where cell numbers were drastically reduced or EPI/PrE ratios were skewed (Figure S3B). However, the most consistent mutant phenotype was the failure of PrE cells to resolve into a single monolayer epithelium (Figure 4A).

For further characterisation of altered ICM morphology, we segmented EPI and PrE tissues as well as individual cells by using fluorescence signal from membrane and lineage markers (Figure 4C). Instead of flattening out beneath the EPI and TE, *Itgb1-/-* PrE tissues and individual PrE cells were less spread and more spherical in shape (Figure 4C-E). Segmented EPI tissues were also more rounded in mutants (Figure S5A). Furthermore, detection of ICM nuclei indicated that *Itgb1-/-* PrE nuclei were more closely clustered around the center of the ICM compared to WT (Figure 4F). These observations indicate that integrin β1 deficiency brings about rounded ICM morphology, stemming from multi-layered PrE tissue as well as shape changes at the level of individual PrE cells.

In addition, the failure to form a spread PrE monolayer was accompanied by disrupted polarity in *Itgb1-/-* embryos. Whereas apical PKCζ intensity peaked at the PrE surface facing the blastocyst cavity, its distribution was broader across the mutant PrE layer compared to WT (Figure S3C) (Saiz et al., 2013). In contrast, PKCζ distribution in the TE was comparable between genotypes (Figure S3D). Similar observations were made with pERM localisation. While WT embryos exhibit bimodal pERM distribution where fluorescence intensity peaks at the apical surface of the polar TE and PrE, *Itgb1-/-* profiles exhibit multiple peaks (Figure 4G). Therefore, although integrin β1 is not required for initial specification of the ICM *in vivo*, it is required for subsequent patterning among EPI and PrE cells inside the blastocyst. Particularly, it is required for the organised formation of a polarised epithelial PrE monolayer. These findings reveal that defects that underlie the reported post-implantation lethality of *Itgb1*$^{-/-}$ embryos in fact arise prior to implantation.

Exogenous ECM leads to EPI cells dwelling on the surface of the ICM

In contrast to TE-ICM specification, subsequent EPI-PrE specification within the ICM is not cell position-dependent since respective cells emerge in a salt-and-pepper pattern (Chazaud et al., 2006; Plusa et al., 2008). Nevertheless, positional information remains pertinent as EPI and PrE cells must resolve into a distinct spatial pattern as described above. Given the requirement for integrin β1 during this latter

process as demonstrated by mutant blastocysts, we tested whether EPI and PrE cells are also receptive to exogenous ECM as positional cues.

Transcription factors NANOG and GATA6 are early markers of EPI and PrE fate, respectively. When ICMs are isolated from blastocysts at E3.5, NANOG- and GATA6-positive nuclei, as well as double-positive nuclei, are intermixed (Figure 5A and 5B). The distance between each nucleus from the centre of the ICM shows no correlation with expression level of cell fate markers (Figure 5C), as expected from a salt-and-pepper pattern.

Following immunosurgery and culture, the salt-and-pepper distribution of fates resolved into a pattern where polarised GATA4-positive PrE surrounded the SOX2-positive EPI (Figure 5D). Positional distinction between EPI and PrE was evident based on cell fate marker expression relative to distance from the ICM centre (Figure 5E). Given the small size of the ICM, correlation coefficient values appeared low, but there was significant positive correlation between GATA4 expression and nuclear distance from the ICM centre, while negative correlation was observed for SOX2 expression. In stark contrast, Matrigel markedly disrupted this spatial arrangement (Figure 5F, top left panel). EPI cells were no longer confined to the interior, but frequently found at the surface. In Matrigel, spatial position could not distinguish the two lineages since PrE cells tend to be closer and EPI cells further from the center of the cultured ICM compared to respective counterparts in KSOM (Figure S4A). In addition, quantitative analysis of fate in peripherally located cells indicated that while the vast majority of outer cells are GATA4-positive in control conditions, a significant portion expresses SOX2 in Matrigel culture (Figure 5G). Furthermore, apical polarity of the ICM surface was replaced by integrin β1 enrichment (Figure 5F, top right panel), as observed from culture of inner cells at the earlier stage.

As with TE-ICM patterning, the effects of Matrigel on EPI-PrE patterning was dependent on integrin β1 activity. Administration of Ha2/5 restored a peripheral polarised PrE layer in the presence of Matrigel (Figure 5F, bottom panels and 5G), as did genetic ablation of *Itgb1* (Figure S4B). These observations demonstrate that ECM-integrin adhesion provides critical positional signals to regulate EPI-PrE patterning within the ICM, consistent with its role in ICM-TE patterning following immunosurgery, and as seen in whole *Itgb1-/-* blastocysts.

Integrin and laminin signal together in the preimplantation embryo

Given our findings, we next sought to identify the extracellular protein component involved in ECM and integrin-mediated position-sensing *in vivo*.

Although laminin itself is a ligand for integrin, integrin β1 is required for the deposition of heterotrimeric laminin into the intercellular space, which in turn can bring its cell surface receptors together (Aumailley et al., 2000; Li et al., 2002). Accordingly, intercellular laminin, as judged by strand-like laminin γ1 signal in the ICM, was diminished in *Itgb1*$^{-/-}$ embryos (Figure 6A). Since the requirement for laminin γ1, encoded by *Lamc1*, is shared by both laminin isoforms (laminin 111 and laminin 511) assembled during the preimplantation stage, our model predicted integrin signalling to be impaired in *Lamc1*$^{-/-}$ embryos.

Examination of *Lamc1-/-* blastocysts revealed that PrE cells failed to resolve into an epithelial monolayer (Figure 6B), despite the number of PrE and EPI cells being comparable to WT (Figure 6C). As predicted, *Lamc1-/-* mutants exhibited diminished integrin β1 activity on the basal side of the PrE (Figure 6D). Linear distribution of active integrin β1 was pronounced at the EPI-PrE boundary in WT ICM. In contrast, however, the signal was punctate and often weak within *Lamc1-/-* ICM.

Furthermore, much like in *Itgb1*$^{-/-}$ counterparts, segmented PrE and EPI tissues were more spherical in *Lamc1-/-* mutants (Figure 6E, S5A), and individual cells were also more rounded compared to WT cells (Figure S5B). PrE cells were more closely clustered around the center of the ICM (Figure 6F), and such failure to form a spread PrE monolayer was accompanied by disrupted apicobasal polarity, as seen in *Itgb1-/-* mutants (Figure S5C-D). Together, the close resemblance between *Itgb1-/-* and *Lamc1-/-* blastocysts supports a model in which intercellular laminin provides crucial positional signals that are interpreted by cells via integrin activity to instruct patterning of the ICM.

The cytoplasmic domain of integrins interacts with a myriad of proteins. Among these, talin plays a key role in linking integrin to the cytoskeleton, and recruits other integrin associated proteins such as vinculin for signalling (Calderwood et al., 1999; Humphries et al., 2007). Indeed, where the active conformation of integrin β1 is enriched on the surface by Matrigel culture, talin signal is also increased, both during ICM induction and in surface-positioned EPI cells (Figure 6G

and 6H). Together, these suggest that talin may be one of the components involved in relaying positional information within the early embryo to affect patterning.

Discussion

During mouse preimplantation development, ICM-TE specification follows an inside-outside pattern, while EPI and PrE cells initially emerge in an intermixed manner before becoming spatially segregated. Despite this difference, however, we show that cells maintain sensitivity to ECM-integrin signals throughout the preimplantation period to gain positional information. Given that altered patterning induced by Matrigel requires integrin $\alpha 6\beta 1$ activity, it follows that laminin, rather than other factors associated with reconstituted ECM, are pertinent for patterning early embryonic cells. This is further supported by the shared phenotype of *Itgb1-/-* and *Lamc1-/-* embryos.

In developing embryos or stem cell systems where cells are yet to differentiate, a myriad of signals must be processed leading up to lineage commitment. During the first lineage segregation, Matrigel is sufficient to drive ICM specification in an integrin-dependent manner, irrespective of cell position. It is worth noting that the ECM cues provided through Matrigel in our setup may be more concentrated than levels found *in vivo*, thereby overriding competing positional signals to drive ICM specification. Yet, integrin activity is not strictly required for initial inside-outside patterning *in vivo*. Given the significance of setting aside cells that will eventually form the embryo proper, other factors, such as the non-integrin laminin receptor dystroglycan, may well be active in the embryonic interior as redundant 'inside' signals (Hynes, 1987; Mui et al., 2016; Williamson et al., 1997). Moreover, single cell gene expression data indicate that other integrins are also present during preimplantation development (Ohnishi et al., 2014). For example, integrins $\alpha v\beta 3$ and $\alpha v\beta 5$ are expressed alongside their cognate ECM ligand, vitronectin (Wayner et al., 1991). The precise contribution by individual ECM components and their receptors during development are subjects for future study.

Our work complements earlier studies in embryonic stem cells that revealed ECM-integrin signals as critical regulators of the undifferentiated state and cell arrangement (Aumailley et al., 2000; Cattavarayane et al., 2015; Li et al., 2002). Given the ubiquity and tissue/stage-dependent complexity of the ECM and its receptors, their role in cell fate specification and pattern formation extends beyond early mouse development (Huang and Ingber, 2005; Humphrey et al., 2014; Walma and Yamada, 2020; Watt and Huck, 2013). Elucidation of their mechanistic contribution to patterning across diverse contexts will be instrumental to how we approach various disease states and design regenerative therapies in the future.

Materials & Methods

Animal work

All animal work was performed in the Laboratory Animals Resources (LAR) facility at the European Molecular Biology Laboratory (EMBL) with permission from the Institutional Animal Care and Use Committee (IACUC) overseeing the operations (IACUC #TH110011). The LAR facility operates according to guidelines and recommendations set by the Federation for Laboratory Animal Science Associations. Mice were maintained in pathogen-free conditions under 12-hour light-dark cycles.

Mouse lines

Wildtype mice were of a F1 hybrid strain from C57BL/6 and C3H (B6C3F1) animals. The following transgenic lines were used in this study : *Itgb1*$^{tm1Efu\ (floxed)}$ (Raghavan et al., 2000), *Lamc1*$^{tmStrl(floxed)}$ (Chen and Strickland, 2003), Zp3-Cre (de Vries et al., 2000). Standard tail genotyping procedures were used to genotype transgenic mice.

To obtain *Itgb1*$^{+/-}$ mice, *Itgb1*$^{tm1Efu\ (floxed)}$ *Zp3-Cre*^{tg} females were crossed with B6C3F1 males. To obtain zygotic *Itgb1*$^{-/-}$ embryos, *Itgb1*$^{+/-}$ females were crossed with *Itgb1*$^{+/-}$ males. To obtain *Lamc1*$^{+/-}$ mice, *Lamc1*$^{tmStrl\ (floxed)}$ *Zp3-Cre*^{tg} females were crossed with B6C3F1 males. To obtain zygotic *Lamc1*$^{-/-}$ embryos, *Lamc1*$^{+/-}$ females were crossed with *Lamc1*$^{+/-}$ males.

Superovulation and dissection of reproductive organs

Superovulation was induced in females 8-22 weeks of age prior to mating to increase the number of preimplantation embryos obtained per mouse. Intraperitoneal injection of 5IU of PMSG (Intervet, Intergonan) and hCG (Intervet, Ovogest 1500) were carried out, with a 48-50 hour interval between the two injections. Each female mouse was put in a cage with a male immediately following hCG injection for mating.

Timing of sacrifice post-hCG injection depends on the developmental stage relevant for the experiment. Given 11AM hormone injections for superovulation, 16-32 cell stage embryos were recovered in the afternoon of E2.5. Early blastocysts were obtained on the morning of E3.5, and for assessment of late blastocysts, these were cultured overnight *in vitro*.

Embryo work

Preimplantation embryos were obtained by flushing the oviduct with a 1ml syringe filled with H-KSOM from the infundibulum. All live embryos were handled under a stereomicroscope (Zeiss, Discovery.v8) equipped with a heating plate (Tokai hit, MATS-UST2). All live embryos were cultured in 10μl microdroplets of KSOM (potassium Simplex Optimized Medium; (Lawitts and Biggers, 1991)) with a mineral oil (Sigma, M8410) overlay inside an incubator (Thermo Fisher Scientific, Heracell 240i) with a 37°C humidified atmosphere of 5% CO2 and 95% air. Micromanipulations outside the incubator were carried out in KSOM containing HEPES (H-KSOM; LifeGlobal, LGGH-050).

Immunosurgery

Zona pellucida were removed from embryos with 3-4 min pronase (0.5% w/v Proteinase K, Sigma P8811, in H-KSOM supplemented with 0.5% PVP-40) treatment at 37°C Subsequently, embryos were incubated in serum containing anti-mouse antibody (Cedarlane, CL2301, Lot no. 049M4847V) diluted 1:3 with KSOM for 30 min at 37°C. Following three brief washes in H-KSOM, embryos were incubated in guinea pig complement (Sigma, 1639, Lot no. SLBX9353) diluted 1:3 with KSOM for

30 min at 37°C. Lysed outer cells were removed by mouth-pipetting with a narrow glass capillary to isolate the inner cells.

Embedding cells in Matrigel

Matrigel mix consists of Matrigel (Corning 356230, lot. 7345012) diluted in DPBS to desired concentration (4.5 mg/ml). Matrigel mix was prepared fresh for each experiment, mixed thoroughly through pipetting, and kept on ice during immunosurgery. Upon completion of immunosurgery, isolated inner cells were promptly resuspended in the mixes, and 15μL droplets were made on 35mm petri dishes (Falcon, 351008). To ensure that cell clusters from different embryos do not stick together, a closed glass capillary was used to space them apart. These petri dishes were inverted to prevent cells sticking to the bottom of the dish, and incubated at 37°C for 30 minutes for the mix to form a gel. After gel formation, 4ml of prewarmed KSOM was gently pipetted into each dish to cover the gel.

To inhibit integrin heterodimer activity in Matrigel-embedded cells, blocking antibodies Ha2/5 and GoH3 that target integrin β1 and α6, respectively, were added to the overlying KSOM medium at a concentration of 10 μg/mL.

Immunostaining

Embryos were fixed in 4% PFA (Sigma, P6148) at room temperature for 15 min, washed 3 times (5 min each) in wash buffer (DPBS-T containing 2% BSA), permeabilised at room temperature for 30 min in permeabilisation buffer (0.5% Triton-X in DPBS; Sigma T8787), washed (3 x 5 min), followed by incubation in blocking buffer (PBS-T containing 5% BSA) either overnight at 4°C or for 2 h at room temperature. Blocked samples were incubated with primary antibodies (Table1) overnight at 4°C, washed (3 x 5 min), and incubated in fluorophore-conjugated secondary antibodies and dyes for 2 hours at room temperature. Stained samples were washed (3 x 5 min), incubated in DAPI solution (Life Technologies, D3571; diluted 1:1000 in DPBS) for 10 min at room temperature. These samples were then transferred into droplets of DPBS overlaid with mineral oil on a 35mm glass bottom dish (MatTek, P356-1.5-20-C) for imaging.

Molecular work

Single embryo genotyping

Individual embryos were mouth pipetted into 200μL PCR tubes containing 10μL of lysis buffer consisting of 200μg/ml Proteinase K in *Taq* polymerase buffer (Thermo Scientific, B38). Lysis reaction took place for 1 hour at 55°C, followed by 10 minutes at 96°C. Resulting genomic DNA was mixed with relevant primers (Table 3) for determination of genotype via PCR

Microscopy and image analyses

Fixed and stained embryos were imaged on the Zeiss LSM780 and LSM880 confocal microscopes. For both systems, a 40X water-immersion C-Apochromat 1.2 NA objective lens was used. Imaging was carried out with the Zen (Zeiss) software interface. Resulting raw images were processed using ImageJ. Further quantification of fluorescence intensities and nuclei/cell counting was performed on either ImageJ or Imaris 9.2.1 (Oxford Instruments) as described below.

Measure of cell circularity

Circularity measurement were obtained by tracing the outline of individual cells on ImageJ following their membrane/actin signal. From each cluster, up to 4-8 TE- and ICM-specified cells were traced across their mid-section. Cells undergoing division were not included, as cells round up during division. The formula for circularity on ImageJ is as follows: *circularity = 4π (area/perimeter^2).*

Detection of nuclei, quantification of their spatial distribution and fluorescence intensity of lineage markers

For detection of nuclei and measure of lineage specification, Imaris Surpass was used, which allowed 3D visualisation of the confocal image data. The 'Add Spots' function was used to detect each nucleus on the DAPI, CDX2, SOX2 or GATA4 channel. Estimated spot (nucleus) diameter was set to 6 μm, and manual

corrections were made for each image as necessary to detect all nuclei. Mean fluorescence intensity of SOX2, CDX2 or GATA4 were measured for each detected nucleus. Spot detection of each nucleus was also used as a cell counter.

xyz coordinates were acquired for each nuclear spot from the statistics tab on Imaris, and used to measure the distance to the center of the ICM. The ICM center coordinates were acquired by calculating the mean between the maximum and minimum values among total ICM cells (EPI and PrE).

Quantification of fluorescence intensity of apicobasal markers

Fluorescence signal intensity of cortical pERM and integrin β1 was used as a measure of apical and basal polarity, respectively. Images of samples stained for these proteins were analysed on ImageJ. To reduce noise, the Gaussian filter was applied to smooth the image. For each z-stack, a mid-slice was selected, and a line was traced along the perimeter of the smoothed image or across cells/tissues of interest. A plot profile along the line was obtained for the pERM, PKCζ, or integrin β1 channel. Individual data points were exported from ImageJ for statistical analysis.

Segmentation of PrE and EPI tissue and subsequent sphericity measurement

Manual segmentation was performed in using the Surface function on Imaris Surpass. Based on fluorescence signals from cell fate markers (GATA4 for PrE and SOX2 for EPI) and membrane dye, PrE and EPI layers were traced for each z-stack of a confocal image acquired at 2μm intervals. Automatic surface rendering on manual traces recreates PrE and EPI segments, and the sphericity of these 3D objects are calculated based on the equation

$$\Psi = \frac{\pi^{1/3}(6V_p)^{2/3}}{A_P}$$

Ψ is sphericity, V*p* is volume of the object, and A*p* is surface area of the object.

Statistical analysis

Statistical analyses and graph generation was performed using the ggplot2 package in R and Microsoft Excel. Comparison of the distribution of fate marker intensities was performed by the Mann-Whitney U test. Differences in cell count, surface enrichment of apicobasal polarity markers, circularity, and ICM/cell sphericity, and distance measurements were assessed using the student's *t*-test (two-sided). Statistical relationship between EPI/PrE fate marker expression and cell position were assessed by Pearson's correlation.

Acknowledgements

We are grateful to members of the Hiiragi Group and Aissam Ikmi for critical comments and suggestions. Karen-Sue Carlson kindly provided *Lamc1* $^{fl/fl}$ mice. We also thank Ramona Bloehs, Stefanie Friese, Lidia Perez, and the Laboratory Animal Resources at EMBL for technical support with mouse work. E.J.Y.K. is supported by the EMBL International PhD Programme, and the Hiiragi Group is supported by EMBL and the European Research Council (ERC Advanced Grant "Self-organising Embryo", grant agreement 742732).

Author contributions

The project was conceived and designed by E.J.Y.K and T.H. L.S. provided expertise and reagents relating to the ECM, particularly laminin, which further guided the design of the project. E.J.Y.K. carried out all experiments, including mouse experiments, imaging and data analysis under the supervision of T.H. E.J.Y.K. wrote the manuscript, which was reviewed and edited by L.S. and T.H. for the final version. T.H. acquired the funding.

Competing interests

The authors declare no competing interests.

References

Alarcon, V. B. (2010). Cell Polarity Regulator PARD6B Is Essential for Trophectoderm Formation in the Preimplantation Mouse Embryo1. *Biology of Reproduction* **83**, 347–358.

Aumailley, M., Pesch, M., Tunggal, L., Gaill, F. and Fässler, R. (2000). Altered synthesis of laminin 1 and absence of basement membrane component deposition in (beta)1 integrin-deficient embryoid bodies. *J Cell Sci* **113 Pt 2**, 259–268.

Bazzoni, G., Shih, D. T., Buck, C. A. and Hemler, M. E. (1995). Monoclonal antibody 9EG7 defines a novel beta 1 integrin epitope induced by soluble ligand and manganese, but inhibited by calcium. *J. Biol. Chem.* **270**, 25570–25577.

Calderwood, D. A., Zent, R., Grant, R., Rees, D. J., Hynes, R. O. and Ginsberg, M. H. (1999). The Talin head domain binds to integrin beta subunit cytoplasmic tails and regulates integrin activation. *J. Biol. Chem.* **274**, 28071–28074.

Cattavarayane, S., Palovuori, R., Tanjore Ramanathan, J. and Manninen, A. (2015). α6β1- and αV-integrins are required for long-term self-renewal of murine embryonic stem cells in the absence of LIF. *BMC Cell Biol.* **16**, 3.

Chan, C. J., Costanzo, M., Ruiz-Herrero, T., Mönke, G., Petrie, R. J., Bergert, M., Diz-Muñoz, A., Mahadevan, L. and Hiiragi, T. (2019). Hydraulic control of mammalian embryo size and cell fate. *Nature* **571**, 112–116.

Chazaud, C., Yamanaka, Y., Pawson, T. and Rossant, J. (2006). Early lineage segregation between epiblast and primitive endoderm in mouse blastocysts through the Grb2-MAPK pathway. *DEVCEL* **10**, 615–624.

Chen, Z.-L. and Strickland, S. (2003). Laminin gamma1 is critical for Schwann cell differentiation, axon myelination, and regeneration in the peripheral nerve. *J Cell Biol* **163**, 889–899.

Cooper, A. R. and MacQueen, H. A. (1983). Subunits of laminin are differentially synthesized in mouse eggs and early embryos. *Developmental Biology* **96**, 467–471.

de Vries, W. N., Binns, L. T., Fancher, K. S., Dean, J., Moore, R., Kemler, R. and Knowles, B. B. (2000). Expression of Cre recombinase in mouse oocytes: A means to study maternal effect genes. *Genesis* **26**, 110–112.

Ducibella, T., Ukena, T., Karnovsky, M. and Anderson, E. (1977). Changes in cell surface and cortical cytoplasmic organization during early embryogenesis in the preimplantation mouse embryo. *J Cell Biol* **74**, 153–167.

Dziadek, M. and Timpl, R. (1985). Expression of nidogen and laminin in basement membranes during mouse embryogenesis and in teratocarcinoma cells. *Developmental Biology* **111**, 372–382.

Fässler, R. and Meyer, M. (1995). Consequences of lack of beta 1 integrin gene expression in mice. *Genes & Development* **9**, 1896–1908.

Fields, B., DeLaForest, A., Zogg, M., May, J., Hagen, C., Komnick, K., Wieser, J., Lundberg, A., Weiler, H., Battle, M. A., et al. (2019). The Adult Murine Intestine is Dependent on Constitutive Laminin-γ1 Synthesis. *Nature Publishing Group* **9**, 19303.

Filimonow, K., Saiz, N., Suwińska, A., Wyszomirski, T., Grabarek, J. B., Ferretti, E., Piliszek, A., Plusa, B. and Maleszewski, M. (2019). No evidence of involvement of E-cadherin in cell fate specification or the segregation of Epi and PrE in mouse blastocysts. *PLoS ONE* **14**, e0212109.

Gattazzo, F., Urciuolo, A. and Bonaldo, P. (2014). Extracellular matrix: a dynamic microenvironment for stem cell niche. *Biochimica et Biophysica Acta* **1840**, 2506–2519.

Guo, G., Huss, M., Tong, G. Q., Wang, C., Li Sun, L., Clarke, N. D. and Robson, P. (2010). Resolution of cell fate decisions revealed by single-cell gene expression analysis from zygote to blastocyst. *Developmental Cell* **18**, 675–685.

Huang, S. and Ingber, D. E. (2005). Cell tension, matrix mechanics, and cancer development. *Cancer Cell* **8**, 175–176.

Humphrey, J. D., Dufresne, E. R. and Schwartz, M. A. (2014). Mechanotransduction and extracellular matrix homeostasis. *Nature Reviews Molecular Cell Biology* **15**, 802–812.

Humphries, J. D., Schofield, N. R., Mostafavi-Pour, Z., Green, L. J., Garratt, A. N., Mould, A. P. and Humphries, M. J. (2005). Dual functionality of the anti-beta1 integrin antibody, 12G10, exemplifies agonistic signalling from the ligand binding pocket of integrin adhesion receptors. *J. Biol. Chem.* **280**, 10234–10243.

Humphries, J. D., Wang, P., Streuli, C., Geiger, B., Humphries, M. J. and Ballestrem, C. (2007). Vinculin controls focal adhesion formation by direct interactions with talin and actin. *J Cell Biol* **179**, 1043–1057.

Hynes, R. O. (1987). Integrins: a family of cell surface receptors. *Cell* **48**, 549–554.

Jouve, C., Iimura, T. and Pourquié, O. (2002). Onset of the segmentation clock in the chick embryo: evidence for oscillations in the somite precursors in the primitive streak. *Development* **129**, 1107–1117.

Klein, G., Langegger, M., Timpl, R. and Ekblom, P. (1988). Role of laminin A chain in the development of epithelial cell polarity. *Cell* **55**, 331–341.

Korotkevich, E., Niwayama, R., Courtois, A., Friese, S., Berger, N., Buchholz, F. and Hiiragi, T. (2017). The Apical Domain Is Required and Sufficient for the First Lineage Segregation in the Mouse Embryo. *DEVCEL* **40**, 235–247.e7.

Larue, L., Ohsugi, M., Hirchenhain, J. and Kemler, R. (1994). E-cadherin null mutant embryos fail to form a trophectoderm epithelium. *Proceedings of the National Academy of Sciences* **91**, 8263–8267.

Lawitts, J. A. and Biggers, J. D. (1991). Optimization of mouse embryo culture media using simplex methods. *J. Reprod. Fertil.* **91**, 543–556.

Leivo, I., Vaheri, A., Timpl, R. and Wartiovaara, J. (1980). Appearance and distribution of collagens and laminin in the early mouse embryo. *Developmental Biology* **76**, 100–114.

Li, S., Harrison, D., Carbonetto, S., Fässler, R., Smyth, N., Edgar, D. and Yurchenco, P. D. (2002). Matrix assembly, regulation, and survival functions of laminin and its receptors in embryonic stem cell differentiation. *J Cell Biol* **157**, 1279–1290.

Lorthongpanich, C., Doris, T. P. Y., Limviphuvadh, V., Knowles, B. B. and Solter, D. (2012). Developmental fate and lineage commitment of singled mouse blastomeres. *Development* **139**, 3722–3731.

Louvet, S., Aghion, J., Santa-Maria, A., Mangeat, P. and Maro, B. (1996). Ezrin becomes restricted to outer cells following asymmetrical division in the preimplantation mouse embryo. *Developmental Biology* **177**, 568–579.

Mendrick, D. L. and Kelly, D. M. (1993). Temporal expression of VLA-2 and modulation of its ligand specificity by rat glomerular epithelial cells in vitro. *Lab Invest* **69**, 690–702.

Miner, J. H., Cunningham, J. and Sanes, J. R. (1998). Roles for laminin in embryogenesis: exencephaly, syndactyly, and placentopathy in mice lacking the laminin alpha5 chain. *J Cell Biol* **143**, 1713–1723.

Miner, J. H., Li, C., Mudd, J. L., Go, G. and Sutherland, A. E. (2004). Compositional and structural requirements for laminin and basement membranes during mouse embryo implantation and gastrulation. *Development* **131**, 2247–2256.

Morin, N. and Sullivan, R. (1994). Expression of fibronectin and a fibronectin-binding molecule during preimplantation development in the mouse. *Hum Reprod* **9**, 894–901.

Mui, K. L., Chen, C. S. and Assoian, R. K. (2016). The mechanical regulation of integrin-cadherin crosstalk organizes cells, signaling and forces. *J Cell Sci* **129**, 1093–1100.

Nishioka, N., Inoue, K.-I., Adachi, K., Kiyonari, H., Ota, M., Ralston, A., Yabuta, N., Hirahara, S., Stephenson, R. O., Ogonuki, N., et al. (2009). The Hippo signaling pathway components Lats and Yap pattern Tead4 activity to distinguish mouse trophectoderm from inner cell mass. *Developmental Cell* **16**, 398–410.

Niwayama, R., Moghe, P., Liu, Y.-J., Fabrèges, D., Buchholz, F., Piel, M. and Hiiragi, T. (2019). A Tug-of-War between Cell Shape and Polarity Controls Division Orientation to Ensure Robust Patterning in the Mouse Blastocyst. *Developmental Cell* **51**, 564–574.e6.

O'Reilly, A. M., Lee, H.-H. and Simon, M. A. (2008). Integrins control the positioning and proliferation of follicle stem cells in the Drosophila ovary. *J Cell Biol* **182**, 801–815.

Ohnishi, Y., Huber, W., Tsumura, A., Kang, M., Xenopoulos, P., Kurimoto, K., Oleś, A. K., Araúzo-Bravo, M. J., Saitou, M., Hadjantonakis, A.-K., et al. (2014). Cell-to-cell expression variability followed by signal reinforcement progressively segregates early mouse lineages. *Nat Cell Biol* **16**, 27–37.

Orkin, R. W., Gehron, P., McGoodwin, E. B., Martin, G. R., Valentine, T. and Swarm, R. (1977). A murine tumor producing a matrix of basement membrane. *The Journal of Experimental Medicine* **145**, 204–220.

Plusa, B., Piliszek, A., Frankenberg, S., Artus, J. and Hadjantonakis, A.-K. (2008). Distinct sequential cell behaviours direct primitive endoderm formation in the mouse blastocyst. *Development* **135**, 3081–3091.

Raghavan, S., Bauer, C., Mundschau, G., Li, Q. and Fuchs, E. (2000). Conditional ablation of beta1 integrin in skin. Severe defects in epidermal proliferation, basement membrane formation, and hair follicle invagination. *J Cell Biol* **150**, 1149–1160.

Rossant, J. and Tam, P. P. L. (2009). Blastocyst lineage formation, early embryonic asymmetries and axis patterning in the mouse. *Development* **136**, 701–713.

Saiz, N., Grabarek, J. B., Sabherwal, N., Papalopulu, N. and Plusa, B. (2013). Atypical protein kinase C couples cell sorting with primitive endoderm maturation in the mouse blastocyst. *Development* **140**, 4311–4322.

Sato, T., Vries, R. G., Snippert, H. J., van de Wetering, M., Barker, N., Stange, D. E., van Es, J. H., Abo, A., Kujala, P., Peters, P. J., et al. (2009). Single Lgr5 stem cells build crypt-villus structures in vitro without a mesenchymal niche. *Nature* **459**, 262–265.

Shirayoshi, Y., Okada, T. S. and Takeichi, M. (1983). The calcium-dependent cell-cell adhesion system regulates inner cell mass formation and cell surface polarization in early mouse development. *Cell* **35**, 631–638.

Smyth, N., Vatansever, H. S., Murray, P., Meyer, M., Frie, C., Paulsson, M. and Edgar, D. (1999). Absence of Basement Membranes after Targeting the LAMC1Gene Results in Embryonic Lethality Due to Failure of Endoderm Differentiation. *J Cell Biol* **144**, 151–160.

Solter, D. and Knowles, B. B. (1975). Immunosurgery of mouse blastocyst. *Proceedings of the National Academy of Sciences* **72**, 5099–5102.

Sonnenberg, A., Janssen, H., Hogervorst, F., Calafat, J. and Hilgers, J. (1987). A complex of platelet glycoproteins Ic and IIa identified by a rat monoclonal antibody. *J. Biol. Chem.* **262**, 10376–10383.

Steinberg, M. S. and Poole, T. J. (1981). Strategies for specifying form and pattern: adhesion-guided multicellular assembly. *Philosophical Transactions of the Royal Society B: Biological Sciences* **295**, 451–460.

Stephenson, R. O., Yamanaka, Y. and Rossant, J. (2010). Disorganized epithelial polarity and excess trophectoderm cell fate in preimplantation embryos lacking E-cadherin. *Development* **137**, 3383–3391.

Streuli, C. H., Schmidhauser, C., Bailey, N., Yurchenco, P., Skubitz, A. P., Roskelley, C. and Bissell, M. J. (1995). Laminin mediates tissue-specific gene expression in mammary epithelia. *J Cell Biol* **129**, 591–603.

Sutherland, A. E., Calarco, P. G. and Damsky, C. H. (1993). Developmental regulation of integrin expression at the time of implantation in the mouse embryo. *Development* **119**, 1175–1186.

Takizawa, M., Arimori, T., Taniguchi, Y., Kitago, Y., Yamashita, E., Takagi, J. and Sekiguchi, K. (2017). Mechanistic basis for the recognition of laminin-511 by α6β1 integrin. *Sci Adv* **3**, e1701497.

Tarkowski, A. K. (1959). Experiments on the Development of Isolated Blastomeres of Mouse Eggs. *Nature* **184**, 1286–1287.

Tarkowski, A. K. and Wróblewska, J. (1967). Development of blastomeres of mouse eggs isolated at the 4- and 8-cell stage. *J Embryol Exp Morphol* **18**, 155–180.

Timpl, R., Rohde, H., Robey, P. G., Rennard, S. I., Foidart, J. M. and Martin, G. R. (1979). Laminin--a glycoprotein from basement membranes. *J. Biol. Chem.* **254**, 9933–9937.

Vinot, S., Le, T., Ohno, S., Pawson, T., Maro, B. and Louvet-Vallée, S. (2005). Asymmetric distribution of PAR proteins in the mouse embryo begins at the 8-cell stage during compaction. *Developmental Biology* **282**, 307–319.

Walma, D. A. C. and Yamada, K. M. (2020). The extracellular matrix in development. *Development* **147**.

Watt, F. M. and Huck, W. T. S. (2013). Role of the extracellular matrix in regulating stem cell fate. *Nature Reviews Molecular Cell Biology* **14**, 467–473.

Wayner, E. A., Orlando, R. A. and Cheresh, D. A. (1991). Integrins alpha v beta 3 and alpha v beta 5 contribute to cell attachment to vitronectin but differentially distribute on the cell surface. *J Cell Biol* **113**, 919–929.

Wicklow, E., Blij, S., Frum, T., Hirate, Y., Lang, R. A., Sasaki, H. and Ralston, A. (2014). HIPPO pathway members restrict SOX2 to the inner cell mass where it promotes ICM fates in the mouse blastocyst. *PLoS Genet.* **10**, e1004618.

Wigger, M., Kisielewska, K., Filimonow, K., Plusa, B., Maleszewski, M. and Suwińska, A. (2017). Plasticity of the inner cell mass in mouse blastocyst is restricted by the activity of FGF/MAPK pathway. *Nature Publishing Group* **7**, 15136.

Williamson, R. A., Henry, M. D., Daniels, K. J., Hrstka, R. F., Lee, J. C., Sunada, Y., Ibraghimov-Beskrovnaya, O. and Campbell, K. P. (1997). Dystroglycan is essential for early embryonic development: disruption of Reichert's membrane in Dag1-null mice. *Hum. Mol. Genet.* **6**, 831–841.

Wolpert, L. (1969). Positional information and the spatial pattern of cellular differentiation. *J. Theor. Biol.* **25**, 1–47.

Yamada, M. and Sekiguchi, K. (2015). Molecular Basis of Laminin-Integrin Interactions. *Curr Top Membr* **76**, 197–229.

Ziomek, C. A. and Johnson, M. H. (1980). Cell surface interaction induces polarization of mouse 8-cell blastomeres at compaction. *Cell* **21**, 935–942.

Figures

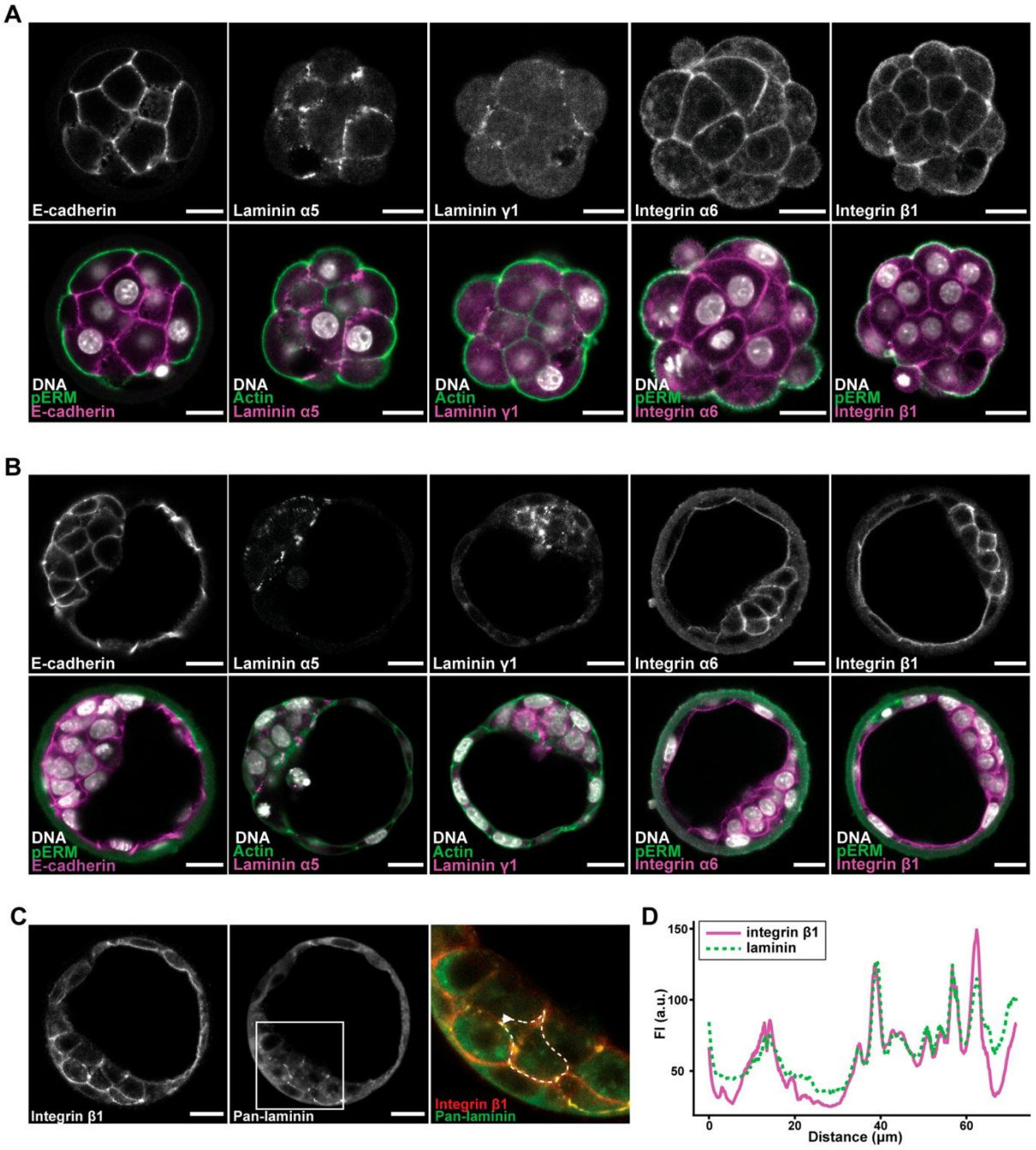

Figure 1. Integrin and laminin are expressed in the morula and colocalise in the blastocyst.

(A and B) Localisation of E-cadherin, laminin chains α5 and γ1, and integrin α6 and β1 subunits in morulae (A) and blastocysts (B). Phosphorylated ezrin, radixin, moesin (pERM) marks the cell-free apical surface of outer cells.

(C) Co-immunostaining for integrin β1 and laminin (non-chain-specific) in the blastocyst marks their shared localisation at the cell-cell interface. Scale bars = 20 μm.
(D) Representative intensity profile of integrin β1 and laminin around an inner cell (marked by dashed white line in (C), arrowhead indicates starting point of measurement).

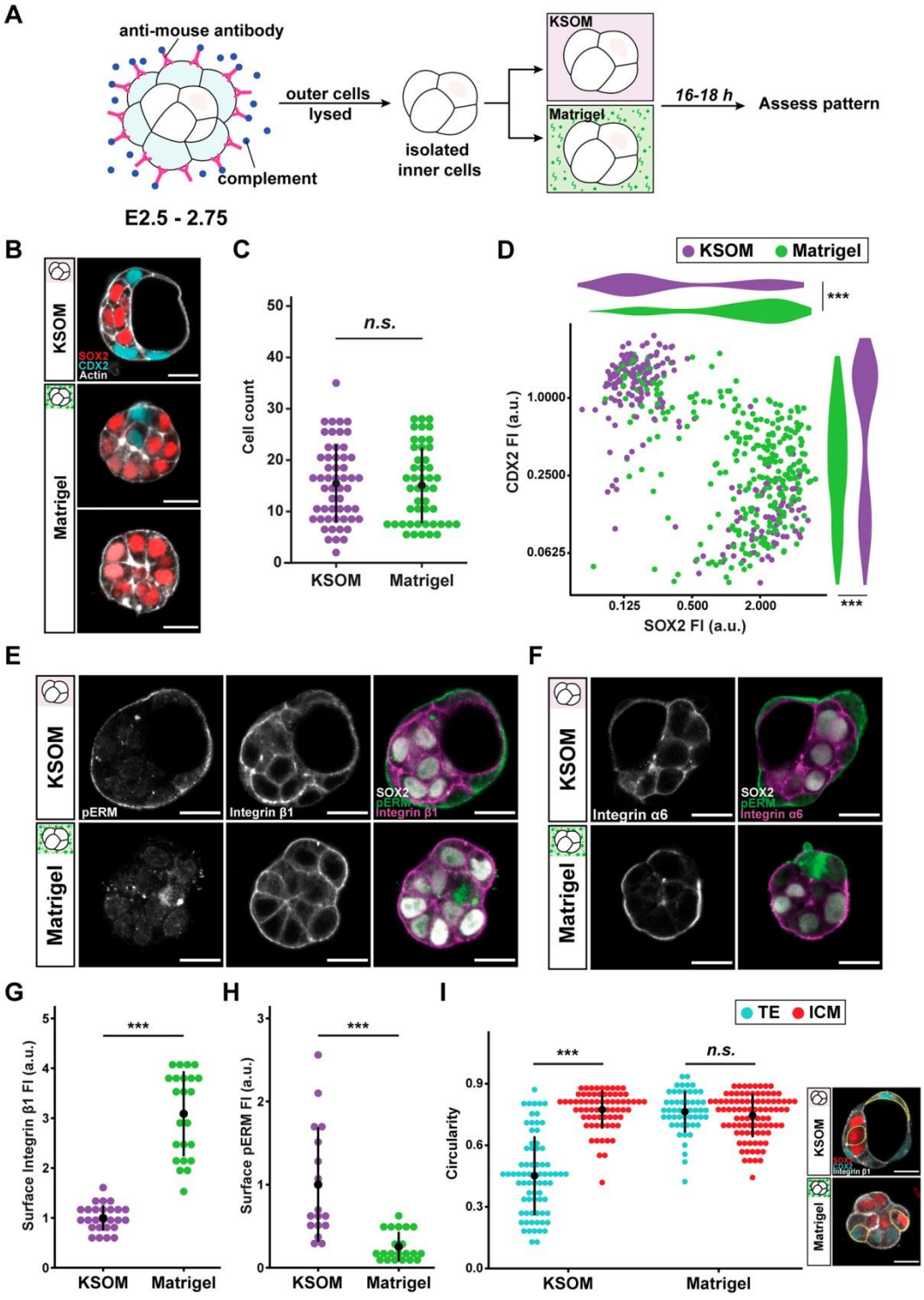

Figure 2. Exogenous ECM drives ICM specification and surface integrin α6β1 enrichment.

(A) Schematic representation of experimental conditions and immunosurgery. Morula stage embryos are recovered prior to ICM specification, and lysis of outer cells leaves behind isolated inner cells. Immediately following immunosurgery, inner

cells are cultured in either standard KSOM mouse embryo media or Matrigel before assessment of patterning.

(B) Representative images of TE-ICM fate specification following immunosurgery and culture in either control KSOM or Matrigel. CDX2 (cyan) marks TE fate while SOX2 (red) marks ICM fate. In a few cases, Matrigel culture induces SOX2 upregulation across the entire cell cluster (bottom panel).

(C) Total cell count after immunosurgery and culture in either KSOM (purple) or Matrigel (green). Each data point represents cell number of inner cell cluster cultured from a single embryo. Student's *t*-test, two-sided. Error bars show mean ± s.d. N = 101 embryos.

(D) Scatterplot and adjacent violin plots show normalised fluorescence intensities of CDX2 and SOX2 measured for each cell cultured in either KSOM (purple) or Matrigel (green). Mann-Whitney U test. N = 43 embryos (n = 912 cells). *** $p < 0.001$

(E and F) Representative images of pERM (apical marker), integrin β1, and integrin α6 localisation in cultured inner cells.

(G and H) Quantification of surface enrichment of integrin β1 and pERM based on fluorescence intensity. Student's *t*-test, two-sided. Error bars show mean ± s.d. N = 49 (F) and N = 38 (G) embryos.

(I) Circularity as a descriptor of cell shape measured for individual TE- and ICM-specified cells across the two culture conditions. Student's *t*-test, two-sided. Error bars show mean ± s.d. N = 46 embryos (n = 288 cells). *** $p < 0.001$. Scale bars = 20 μm.

See also Figure S1.

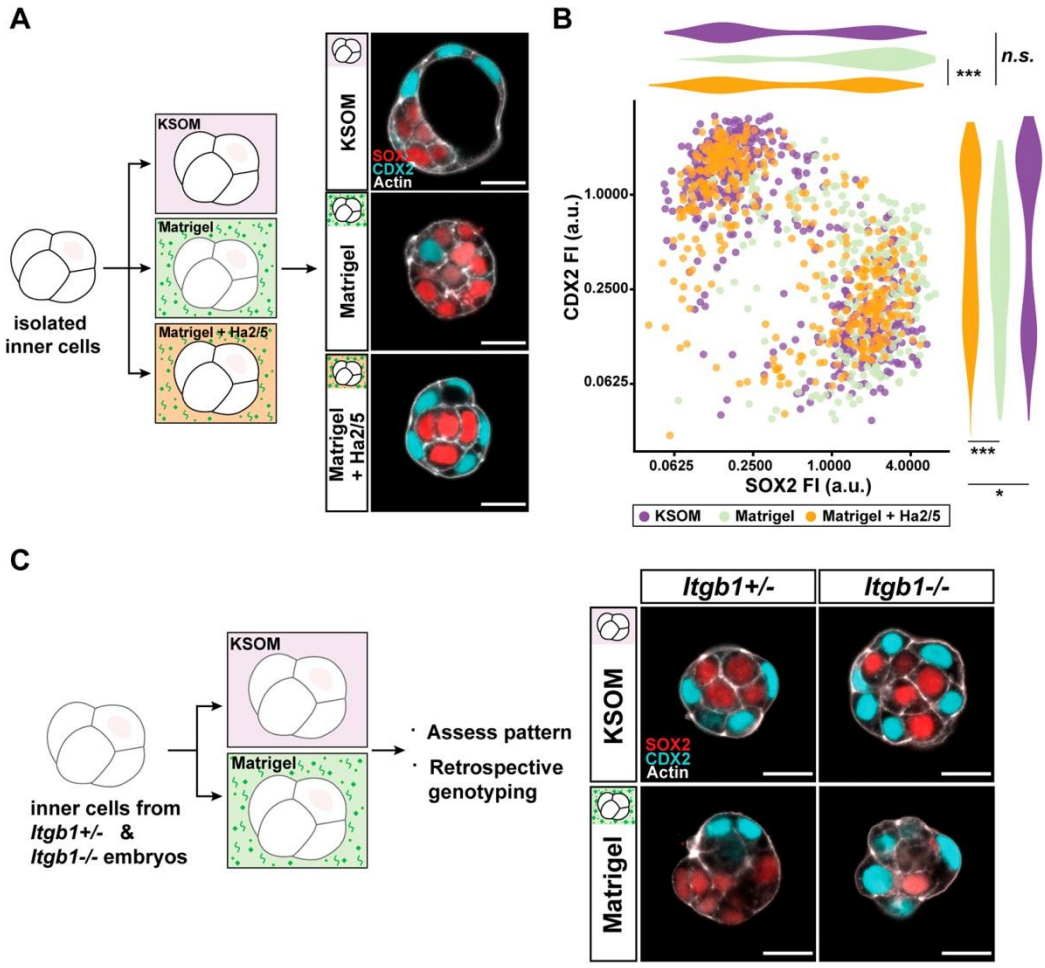

Figure 3. ICM induction by Matrigel is dependent on integrin β1 activity.

(A) Schematic representation of experimental conditions and representative images of TE-ICM patterning upon administration of integrin β1 function-blocking antibody, Ha2/5 (10μg/ml) with Matrigel.

(B) Scatterplot and adjacent violin plots show normalised fluorescence intensities of CDX2 and SOX2 measured for each cell cultured in either KSOM (purple), Matrigel only (light green) or Matrigel with Ha2/5 (orange). Mann-Whitney U test. Plot represents data combined from N = 93 embryos (n= 1332 cells). Data for KSOM and Matrigel are duplicated from Figure 3D for ease of comparison. * $p < 0.05$, *** $p < 0.001$.

(C) Schematic representation of experimental conditions and representative images of inner cells isolated from *Itgb1* transgenic embryos cultured in either KSOM or Matrigel. Each sample is genotyped retrospectively to identify *Itgb1*$^{-/-}$ samples. *Itgb1*+/- samples serve as littermate controls. N = 25 embryos (14 *Itgb1*$^{+/-}$ and 11 *Itgb1*$^{-/-}$). Scale bars = 20 μm. See also Figure S2.

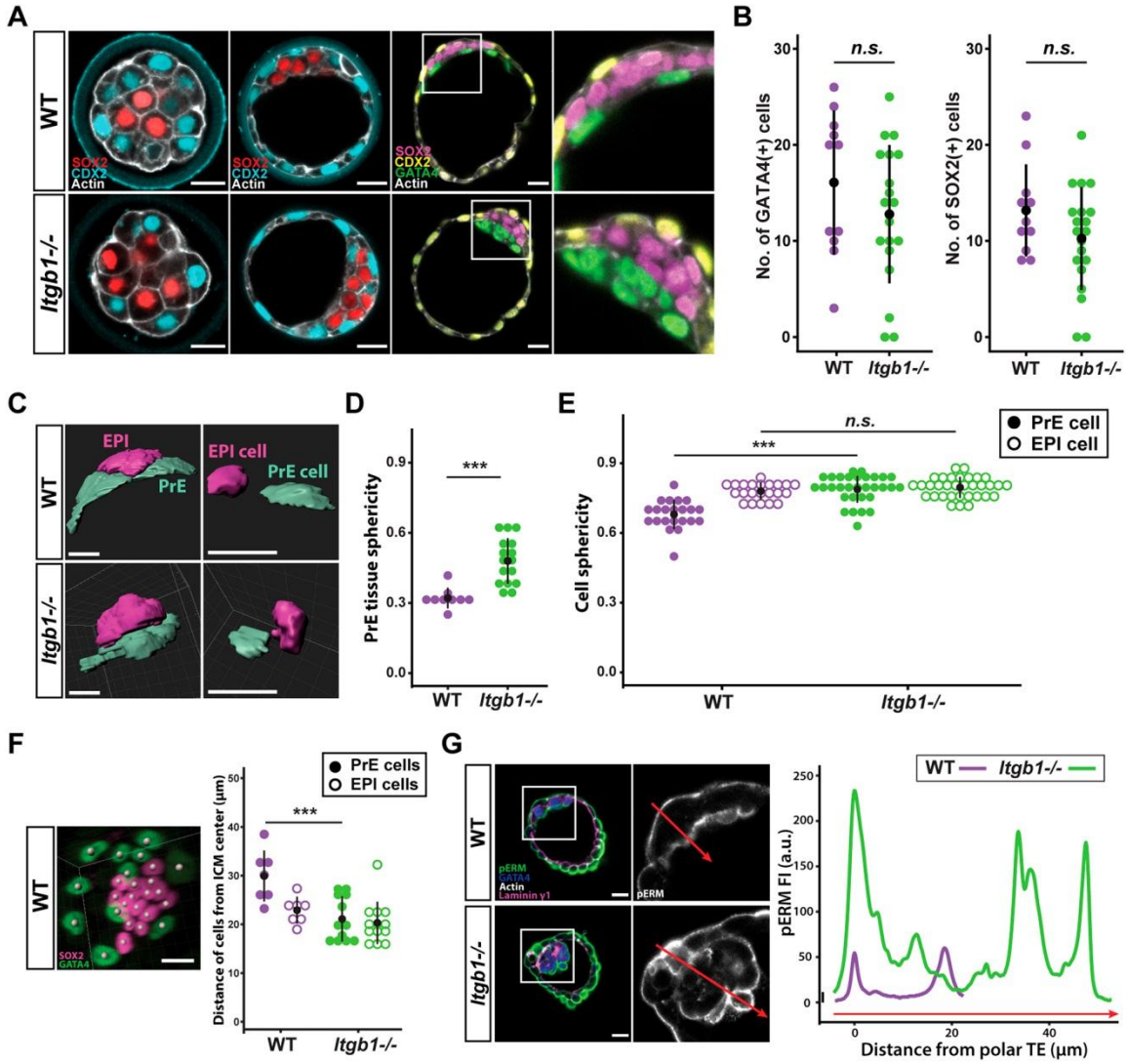

Figure 4. EPI-PrE patterning in the late blastocyst *in vivo* requires integrin β1.

(A) Representative images of lineage patterning in preimplantation stage WT and *Itgb1*$^{-/-}$ embryos through morula, early and late blastocyst stages.

(B) Cell count of GATA4-expressing PrE cells and SOX2-expressing EPI cells within the ICM of WT and *Itgb1*$^{-/-}$ late blastocysts. Student's *t*-test, two-sided. Error bars show mean ± s.d. N=31 embryos (11 WT, 20 *Itgb1*$^{-/-}$).

(C) Representative images of segmented PrE (cyan) and EPI (magenta), as well as individual segmented cells in E4.0 blastocysts on Imaris.

(D-E) Sphericity of PrE tissue and individual cells of the ICM, acquired from segmented surfaces, are compared across WT and *Itgb1-/-* blastocysts at E4.0. Student's *t*-test, two-sided. Error bars show mean ± s.d. *** $p < 0.001$. N = 25 embryos (D) and 108 cells from 17 embryos (E).

(F) Representative image of EPI(SOX2) and PrE(GATA4) nuclei detected in 3D on Imaris. Individual *xyz* coordinates of detected spots are used to calculate the distance of each nucleus from the center of the ICM. On the plot, each dot represents average distance value from all PrE or EPI cells from one embryo. Student's *t*-test, two-sided. Error bars show mean per embryo ± s.e.m. N = 25 embryos. *** $p < 0.001$

(G) Representative image of morphology and apical polarity of the ICM in WT and *Itgb1*$^{-/-}$ blastocysts at E4.0. Accompanying intensity profile shows distribution of pERM across the ICM along the red line of interest. Scale bars = 20 μm. See also Figure S3.

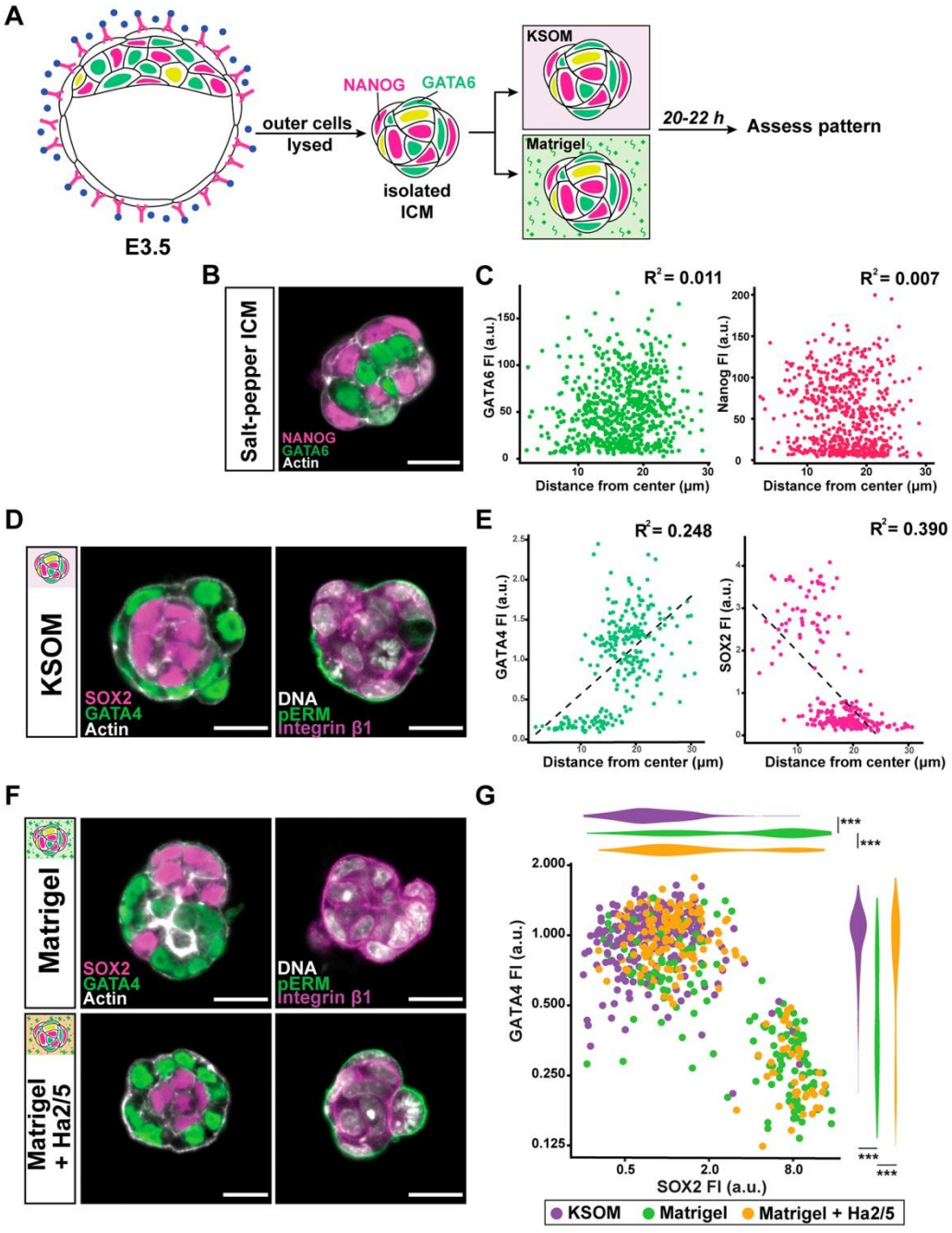

Figure 5. EPI-PrE patterning is sensitive to Matrigel and integrin β1 activity.

(A) Schematic representation of experimental conditions with immunosurgery of blastocysts. Blastocysts are subjected to immunosurgery to isolate salt-and-pepper stage ICMs. Isolated ICMs are cultured in either KSOM or Matrigel before assessment of patterning.

(B) Representative image of an isolated salt-and-pepper ICM expressing early EPI marker NANOG (magenta) and early PrE marker GATA6 (green).

(C) Scatterplots showing fluorescence intensities of GATA6 and NANOG in relation to cell position within an isolated salt-and-pepper ICM. Position is measured as distance

between each nucleus and the centre of the ICM. Pearson's correlation. ICMs from N = 28 embryos (n = 658 cells).

(D) Representative images of EPI-PrE arrangement and apicobasal polarity of ICMs following culture in KSOM. SOX2 (magenta) marks EPI cells, and GATA4 (green) marks PrE cells on left panel.

(E) Scatterplots showing fluorescence intensities of GATA4 and SOX2 in relation to cell position following culture of ICMs in KSOM. Pearson's correlation. $p < 0.0001$ for both GATA4 and SOX2. ICMs from N = 35 embryos (n = 765 cells).

(F) Representative images of EPI-PrE spatial arrangement and apicobasal polarity of ICMs following culture in Matrigel or Matrigel with integrin β1 function-blocking antibody, Ha2/5 (10μg/ml). Scale bars = 20 μm.

(G) Scatterplot and adjacent violin plots show normalised fluorescence intensities of GATA4 and SOX2 measured for each cell cultured in KSOM (purple), Matrigel (green), or Matrigel with Ha2/5 (orange). Mann-Whitney U test. Plot represents data from ICMs from N = 59 embryos (n = 1664 cells). *** $p< 0.001$. See also Figure S4.

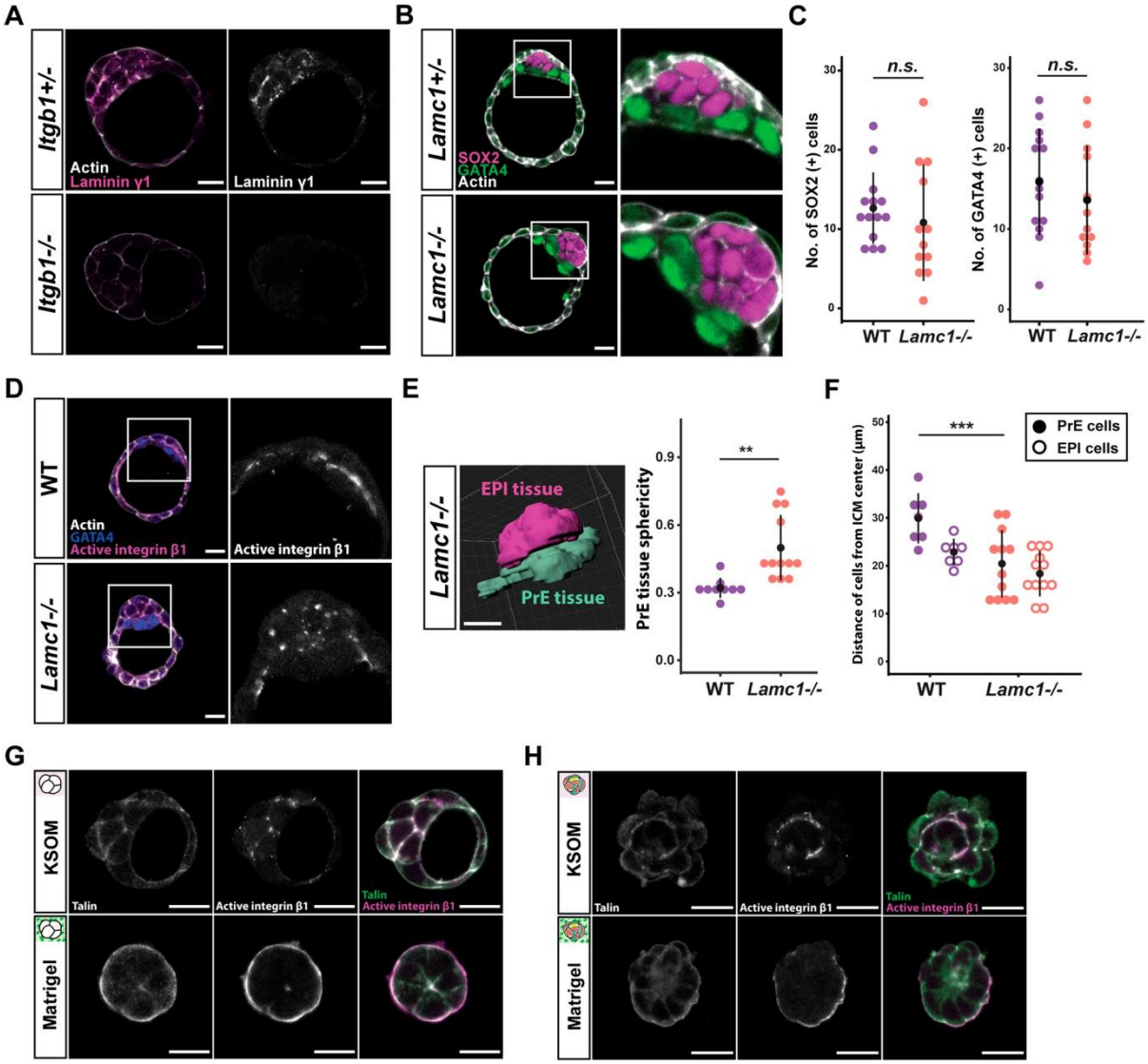

Figure 6. Integrin and laminin signal together in the preimplantation embryo.

(A) Representative images of laminin γ1 chain localisation in *Itgb1*$^{+/-}$ or *Itgb1*$^{-/-}$ blastocysts at E4.0. *Itgb1*$^{+/-}$ embryos serve as littermate controls.

(B) Representative images of EPI-PrE patterning within the ICM of WT and *Lamc1*$^{-/-}$ blastocysts at E4.0. *Lamc1*$^{+/-}$ embryos serve as littermate controls.

(C) Cell count of GATA4-expressing PrE cells and SOX2-expressing EPI cells within the ICM of WT and *Lamc1*$^{-/-}$ blastocysts. Student's *t*-test, two-sided. Error bars show mean ± s.d. N=26 embryos (14 WT, 12 *Lamc1*$^{-/-}$).

(D) Representative images show distribution of active integrin β1 (9EG7 antibody) within the ICM of WT and *Lamc1*$^{-/-}$ blastocysts at E4.0.

(E) Representative image of segmented PrE and EPI tissues in a *Lamc1-/-* blastocyst at E4.0 on Imaris. Plot displays sphericity of PrE tissue, calculated from segmented

surfaces. Error bars show mean ± s.d. Student's *t*-test, two-sided. N = 22 embryos. ** $p<0.01$.

(F) Dot plot shows distance of PrE and EPI nuclei from the center of the ICM. Each dot represents average distance value from all PrE or EPI cells from one embryo. Error bars show mean per embryo ± s.e.m. Student's *t*-test, two-sided. N = 38 embryos. *** $p < 0.001$.

(G-H) Representative images of localisation of talin and the active conformation of integrin β1 (9EG7 antibody), following immunosurgery at either E2.5 (G) or E3.5 (H) and culture in KSOM or Matrigel. Scale bars = 20 μm.

Table 1. Primary antibodies

Epitope	Host	Catalogue #	Company	Dilution
aPKC (PKCζ)	Rabbit	sc-216	Santa Cruz Biotechnology	1:200
CDX2	Mouse	MU392A-UC	Biogenex	1:200
E-cadherin	Rat	U3254	Sigma Aldrich	1:100
GATA4	Goat	AF2606	R&D Systems	1:200
GATA6	Goat	AF1700	R&D Systems	1:200
Integrin α6 (GoH3)	Rat	555734	BD Pharmingen	1:100
Integrin β1	Rat	MAB1997	Millipore	1:100
Integrin β1 (Ha2/5)	Rat	555002	BD Pharmingen	1:100
Integrin β1 (active, 9EG7)	Rat	553715	BD Pharmingen	1:100
Integrin β1 (active, 12G10)	Mouse	sc-59827	Santa Cruz Biotechnology	1:100
Laminin (non-chain specific)	Rabbit	NB300-14422	Novus Biologicals	1:100
Laminin α5	Rat	n/a	Gift from Lydia Sorokin	N/A
Laminin β1	Rat	n/a	Gift from Lydia Sorokin	N/A
Laminin γ1	Rat	n/a	Gift from Lydia Sorokin	N/A
NANOG	Rabbit	RCAB002P-F	ReproCELL, Inc	1:200
YAP1	Mouse	H00010413-M01	Abnova	1:100
Phospho-ERM	Rabbit	3726	Cell Signaling Technology	1:200
Sox-2 (D9B8N)	Rabbit	23064	Cell Signaling Technology	1:200

Table 2. Secondary antibodies and dyes

Fluorophore	Target	Host	Catalogue #	Company	Dilution
Alexa Fluor 488	Goat IgG	Donkey	A11055	Life Technologies	1:200
Alexa Fluor 488 Plus	Rabbit IgG	Donkey	A32790	ThermoFisher	1:200
Alexa Fluor 546	Rabbit IgG	Donkey	A10040	ThermoFisher	
Cy5	Mouse IgG	Donkey	715-175-150	Jackson ImmunoResearch	1:200
Cy5	Rat IgG	Donkey	712-175-153	Jackson ImmunoResearch	1:200
DAPI	(DNA)	-	D3571	Life Technologies	1:1000
Rhodamine phalloidin	(Actin)	-	R415	Invitrogen	1:200

Table 3. Sequence of genotyping primers

Mouse line/locus	Primer 1	Primer 2	Primer 3
Itgb1 deleted	TGAATATGGGCTT GGCAGTTA	CCACAACTTTCCCA GTTAGCTCTC	
Itgb1 tm1Efu (floxed)	CGGCTCAAAGCA GAGTGTCAGTC	CCACAACTTTCCCA GTTAGCTCTC	
Lamc1 deleted/ *Lamc1* tmStrl (floxed)	AAA GAA GCA GAG TGT GGG GG	TGG CCT TTT CAA CCC TGG AA	GCC TTC TAT CGC CTT CTT GAC
ZP3 Cre	TGCTGTTTCACTG GTTGTGCGGCG	TGCCTTCTCTACAC CTGCGGTGCT	

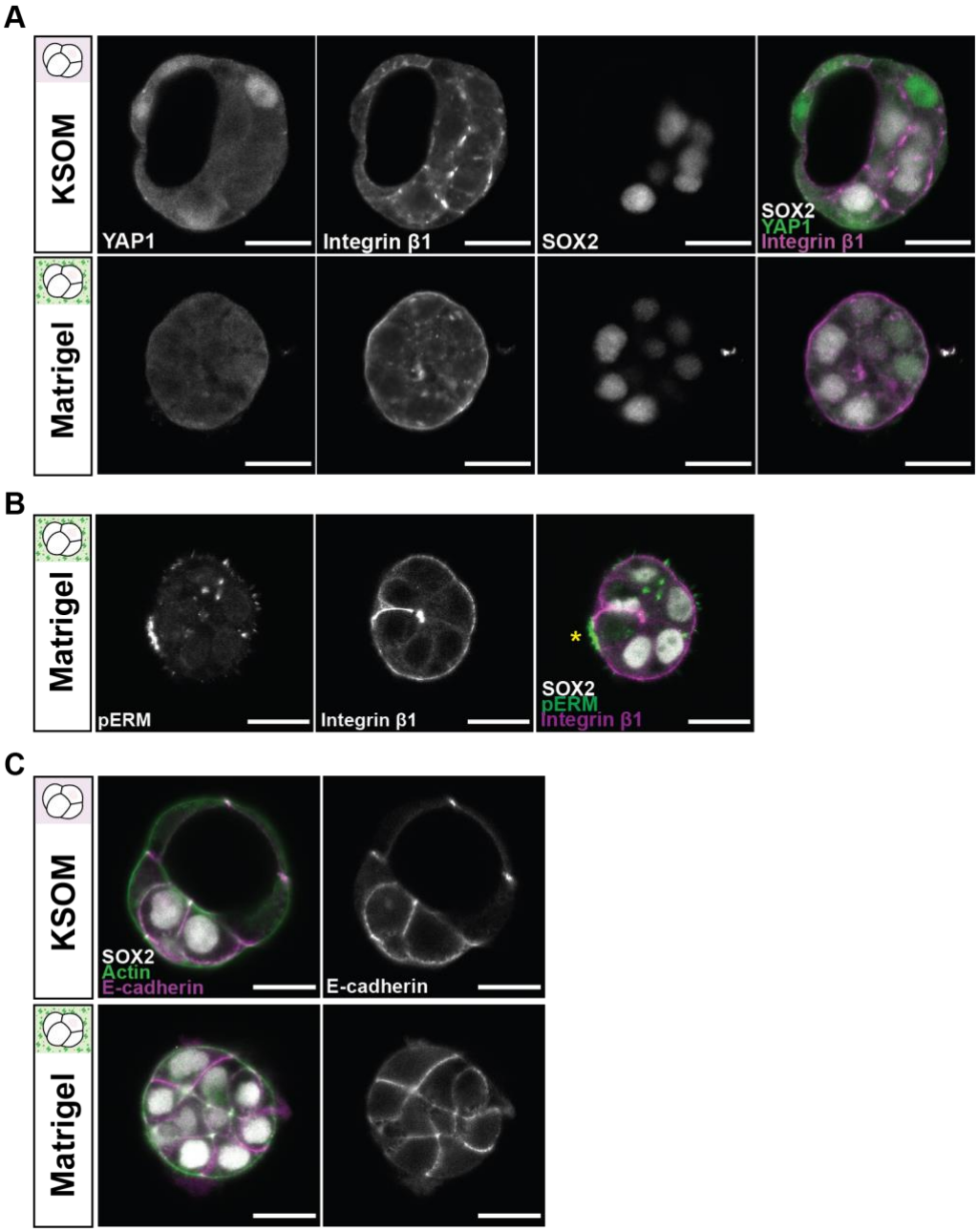

Fig. S1. Exogenous ECM drives Hippo signalling and suppresses apical polarity. Related to Figure 2. (A) Representative images of TE-ICM fate specification and integrin β1 distribution among cells following immunosurgery and culture in KSOM or Matrigel. SOX2 marks ICM fate while nuclear YAP1 is characteristic of TE cells.
(B) Partial enrichment of pERM on the surface of isolated cells cultured in Matrigel. The cell with the patch of pERM signal (*) is SOX2-negative.
(C) Representative images of E-cadherin localisation in isolated cells following culture in KSOM or Matrigel. Scale bars = 20 μm.

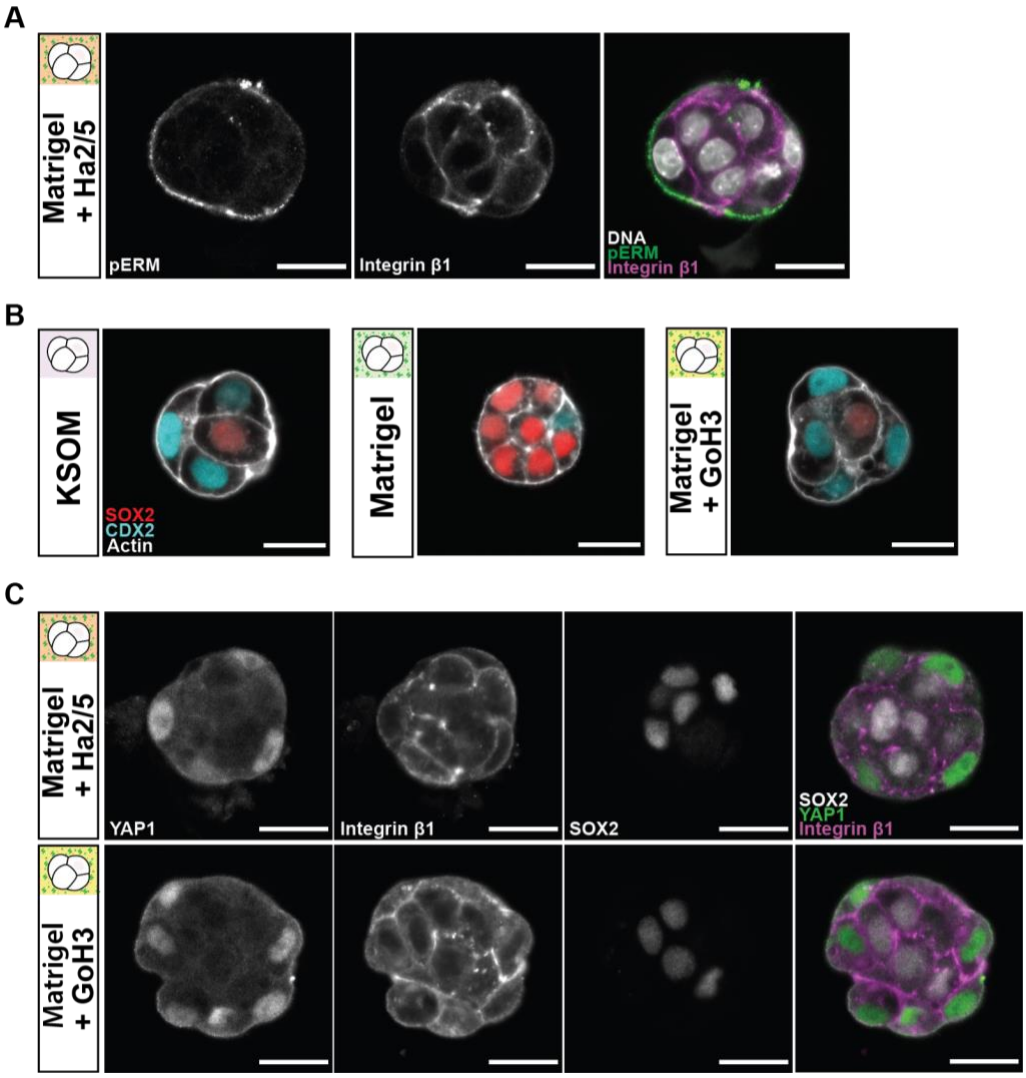

Fig. S2. Integrin α6β1 inhibition restores inside-outside patterning to Matrigel-cultured cells. Related to Figure 3. (A) Representative images of apicobasal polarity in cells cultured in Matrigel with integrin β1 function-blocking antibody Ha2/5 (10 μg/ml). Phosphorylated ERM (pERM) proteins mark apical domain.
(B) Representative images of TE-ICM fate specification following culture in KSOM, Matrigel, or Matrigel with integrin α6 function-blocking antibody GoH3 (10 μg/ml).
(C) Representative images of inside-outside patterning following culture in Matrigel with either Ha2/5 or GoH3. In addition to SOX2 expression, differential localisation of YAP1 distinguishes TE and ICM fate, as YAP1 is nuclear localised in TE cells. Scale bars = 20 μm.

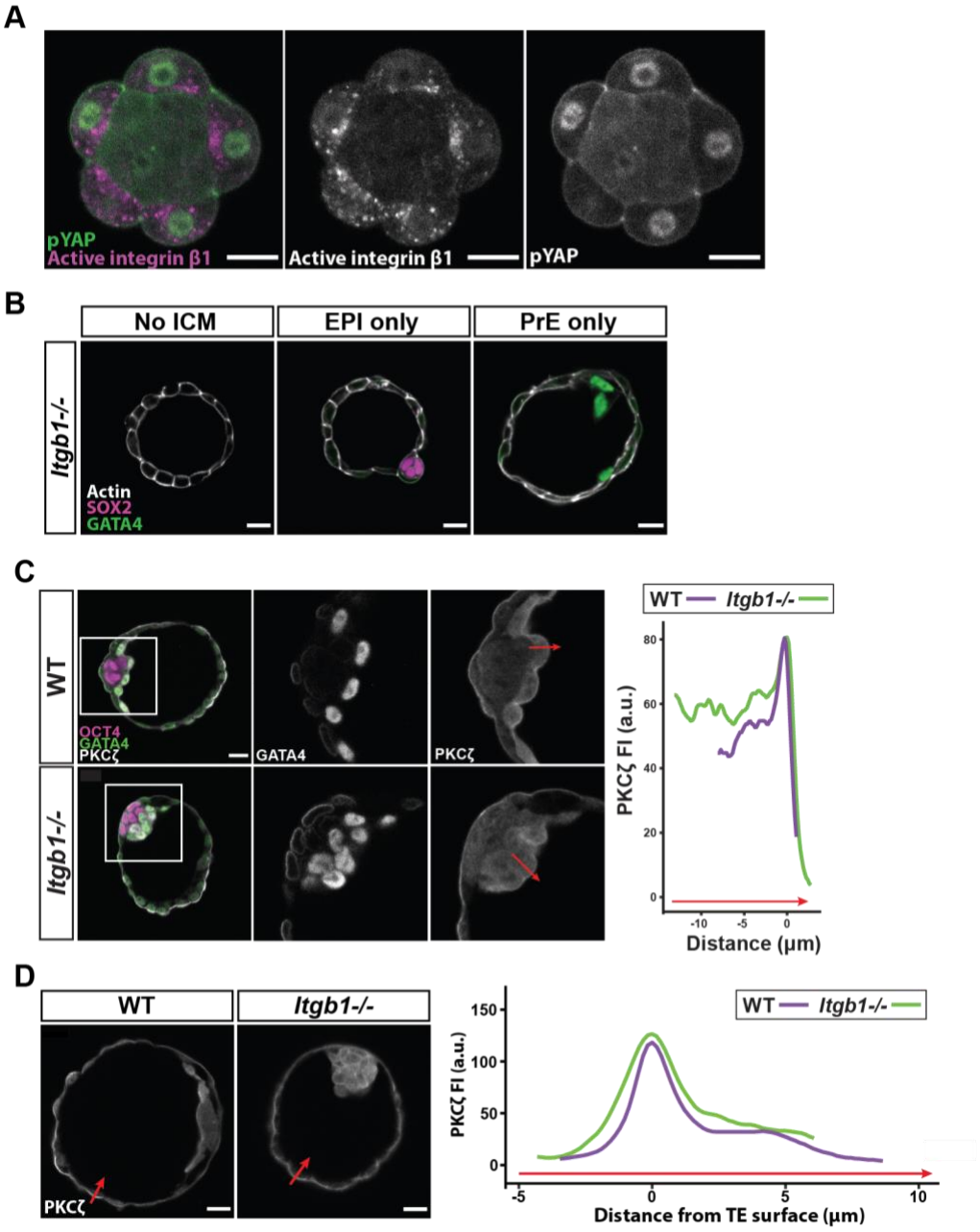

Fig. S3. EPI-PrE patterning in the late blastocyst *in vivo* requires integrin β1. Related to Figure 4.

(A) Representative images show localisation of the active conformation of integrin β1 (12G10 antibody) in the morula stage embryo. Phosphorylated YAP (pYAP) signal distinguishes inside and outside cells, as inside cells exhibit cytoplasmic pYAP localisation.

(B) Images of *Itgb1*$^{-/-}$ blastocysts with severe disruption of ICM.

(C) Representative images show PKCζ distribution across the PrE in WT and *Itgb1*$^{-/-}$ blastocysts at E4.0, followed by plot profile of fluorescence intensity along line of interest across the PrE layer (red arrow).

(D) Representative images of PKCζ distribution in WT and *Itgb1*$^{-/-}$ blastocysts at E4.0, followed by profile plot of fluorescence intensity along line of interest (red arrow) across the TE. Plot profiles are aligned based on the point of maximum PKCζ intensity at the apical surface of TE surface (distance "0").

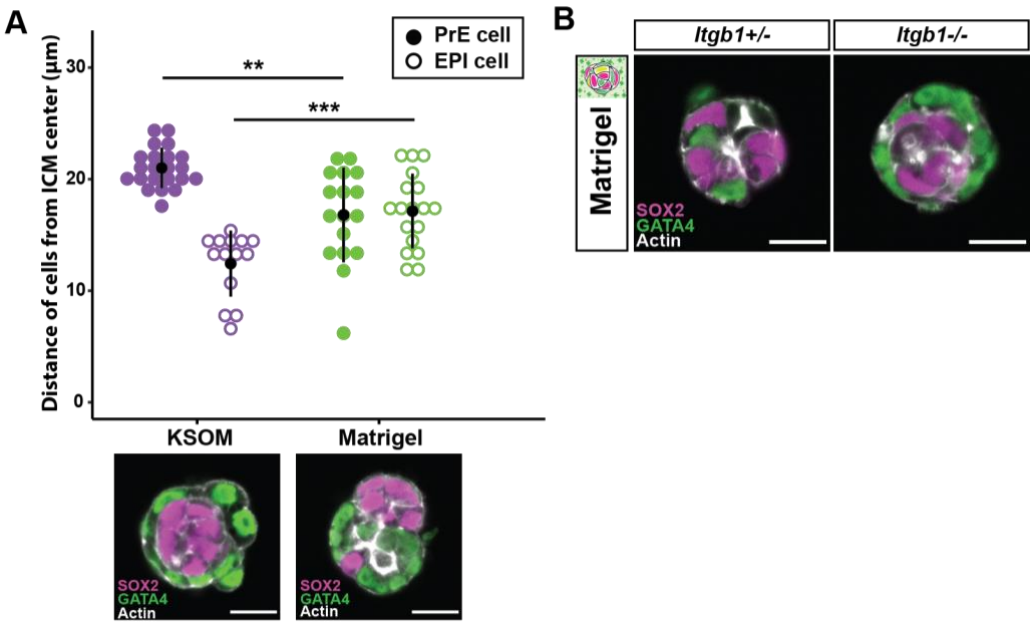

Fig. S4. Matrigel disrupts spatial arrangement of EPI/PrE cells in isolated ICMs. Related to Figure 5.

(A) Distance of PrE and EPI cells from the center of the ICM cultured in either KSOM or Matrigel. Distance data are from representative samples displayed beneath the plot (same as images from Figure 5D and 5F).

(B) Representative images of ICMs isolated from E3.5 *Itgb1* transgenic embryos and cultured in either Matrigel. ICMs from *Itgb1+/-* embryos serve as littermate controls. SOX2 marks EPI cells, and GATA4 marks PrE cells. Scale bars = 20 μm.

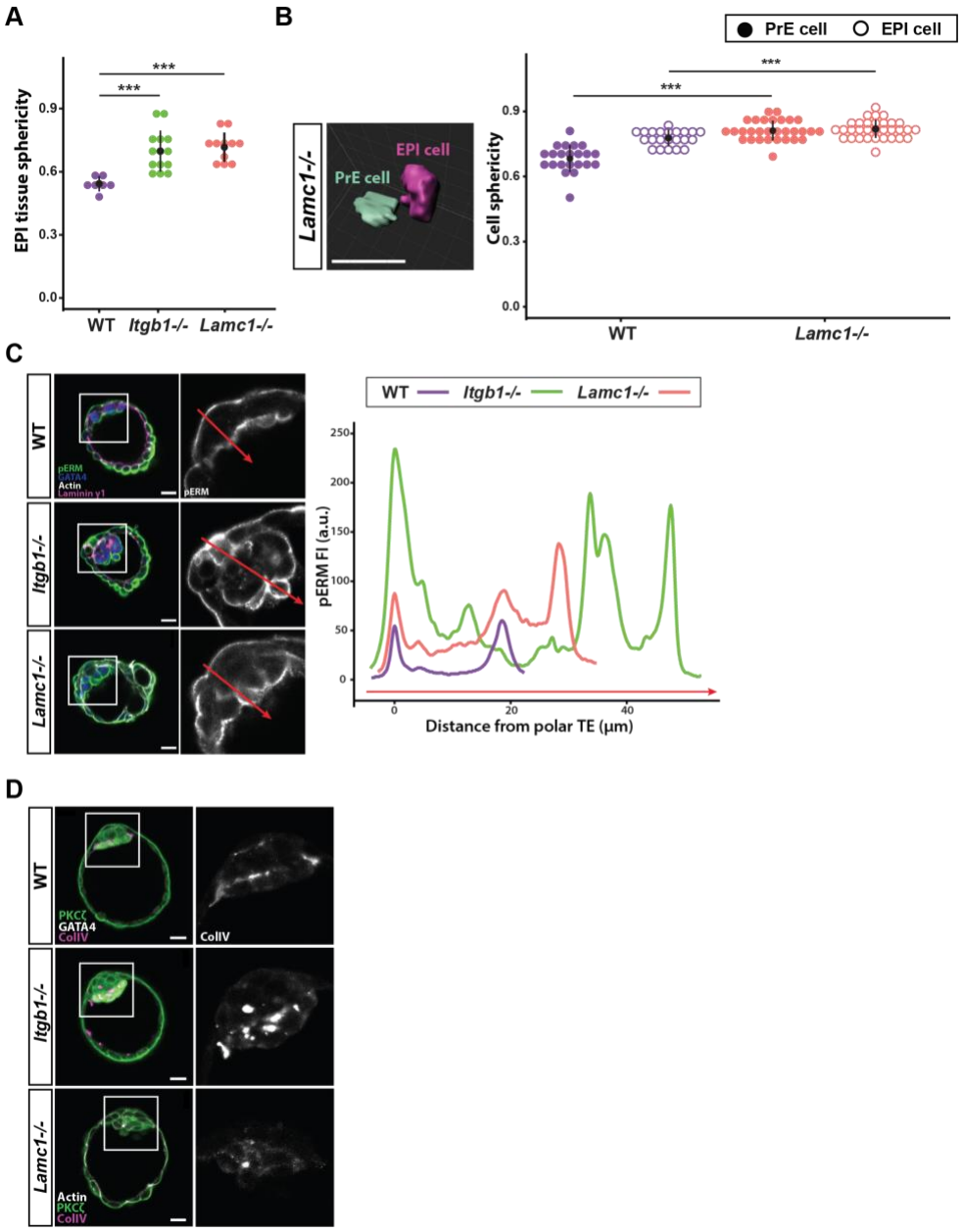

Fig. S5. *Lamc1-/-* embryos share phenotype with *Itgb1-/-* embryos at E4.0. Related to Figure 6.

(A) Sphericity of segmented EPI tissues from WT, *Itgb1-/-*, and *Lamc1-/-* blastocysts at E4.0. Error bars show mean ± s.d. Student's *t*-test, two-sided. N = 32 embryos. *** $p < 0.001$.

(B) Representative image of individual *Lamc1-/-* PrE and EPI cells segmented on Imaris. Dot plot displays sphericity measured from individual segmented surfaces. Error bars show mean ± s.d. Student's *t*-test, two-sided. N = 106 cells from 17 embryos. *** $p < 0.001$.

(C) Representative image of morphology and apical polarity of the ICM in WT, *Itgb1*$^{-/-}$, and *Lamc1-/-* blastocysts at E4.0. Accompanying intensity profile shows distribution of pERM across the ICM along the red line of interest. Data for WT and *Itgb1-/-* are duplicated from Figure 4G for ease of comparison with *Lamc1-/-* mutants.

(D) Representative images show distribution of basal collagen IV in WT, *Itgb1-/-* and *Lamc1-/-* embryos at E4.0. Scale bars = 20 μm.

Table S1.

Click here to download Table S1